An Investigation of Optimal Vehicle Maneuvers for Different Road Conditions ⋆

Björn Olofsson * **Kristoffer Lundahl** ** **Karl Berntorp** * **Lars Nielsen** **

* *Department of Automatic Control, Lund University,*
SE–221 00 Lund, Sweden, `firstname.lastname@control.lth.se.`
** *Department of Electrical Engineering, Linköping University,*
SE–581 83 Linköping, Sweden, `firstname.lastname@liu.se.`

Abstract: We investigate optimal maneuvers for road-vehicles on different surfaces such as asphalt, snow, and ice. The study is motivated by the desire to find control strategies for improved future vehicle safety and driver assistance technologies. Based on earlier presented measurements for tire-force characteristics, we develop tire models corresponding to different road conditions, and determine the time-optimal maneuver in a hairpin turn for each of these. The obtained results are discussed and compared for the different road characteristics. Our main findings are that there are fundamental differences in the control strategies on the considered surfaces, and that these differences can be captured with the adopted modeling approach. Moreover, the path of the vehicle center-of-mass was found to be similar for the different cases. We believe that these findings imply that there are observed vehicle behaviors in the results, which can be utilized for developing the vehicle safety systems of tomorrow.

1. INTRODUCTION

Motivated by the desire to devise improved safety systems for vehicles and driver assistance technologies, development of mathematical models and model-based control strategies for optimal vehicle maneuvers in time-critical situations have emerged as powerful tools during the past years. Even though the solution to an optimal control problem depends on the particular choice of model and cost function, the fundamental behavior and control strategies found by optimization can be used as inspiration for, or be integrated in, future safety-systems.

One step towards this is to study the behavior of a vehicle in a time-critical maneuver under varying road conditions, *e.g.*, dry asphalt and snow. Therefore, we investigate a hairpin maneuver, see Fig. 1. The objective is to perform the maneuver in minimum time, while fulfilling certain constraints on the control inputs and internal states of the vehicle. This means that the vehicle, and in particular the tires, are performing at their limits. We utilize established vehicle and tire modeling principles, and present a model-based optimal control problem with the solution thereof for different road conditions. In addition, we investigate how to scale the tire models for different surfaces. By this study, it is plausible that the understanding of vehicle dynamics in extreme situations under environmental uncertainties is increased.

Optimal control problems for vehicles in time-critical situations have been studied in the literature previously, see (Velenis and Tsiotras, 2005; Velenis, 2011) for different examples. In (Kelly and Sharp, 2010) the time-optimal race-car line was investigated, and in (Sharp and Peng, 2011) a survey on existing vehicle dynamics applications of optimal control theory was presented. Other examples are (Sundström et al., 2010; Funke

Fig. 1. An example of a partly snow-covered hairpin turn.

et al., 2012). We presented a method for determining optimal maneuvers and a subsequent comparison using different methods for tire modeling in (Berntorp et al., 2013). Further, a comparison of optimal maneuvers with different chassis models was treated in (Lundahl et al., 2013). Scaling of nominal tire models for different surfaces was discussed and experimentally verified in (Braghin et al., 2006). Even though the vehicle and tire models utilized in this paper are similar to those presented in the mentioned references, previous research approaches focus on a particular vehicle model on a specific surface. Comparisons of optimal control maneuvers for different road conditions have been made, see (Chakraborty et al., 2011), but are limited to varying the friction coefficient, and we show that important tire-force characteristics might be neglected with that approach. To the best of our knowledge, no comprehensive approach to perform comparisons of optimal control maneuvers for different road conditions has been made, which motivates the study presented here.

2. MODELING

The vehicle dynamics is modeled with an extended single-track model together with a wheel model and a Magic Formula tire model.
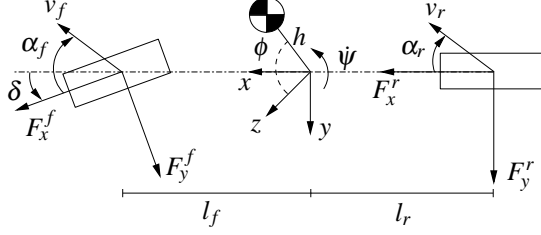
Fig. 2. The single-track model including roll motion about the x-axis, resulting in a four degrees-of-freedom chassis model.

2.1 Vehicle Modeling

The vehicle model considered is a single-track model (Kiencke and Nielsen, 2005; Isermann, 2006) with lumped right and left wheels. In addition, a rotational degree of freedom about the x-axis—i.e., the roll—has been added. The coordinate system is located in the ground plane, at the xy-coordinates of the center of mass for zero roll angle, see Fig. 2. The motivation for the single-track model is twofold; first, we are aiming for models possible to utilize together with dynamic optimization algorithms. Second, we want to investigate what properties of a vehicle that can be captured with this comparably simple model. The roll dynamics is of importance, in order to verify that the vehicle is not overbalancing in the aggressive hairpin maneuver. The model does not incorporate load transfer, but the effect of this has previously been investigated in (Lundahl et al., 2013). The model equations are

$$m\dot{v}_x = F_X + mv_y\dot{\psi} - mhs_\phi\ddot{\psi} - 2mhc_\phi\dot{\phi}\dot{\psi}, \tag{1}$$

$$m\dot{v}_y = F_Y - mv_x\dot{\psi} - mhs_\phi\dot{\psi}^2 + mh\ddot{\phi}c_\phi - m\dot{\phi}^2hs_\phi, \tag{2}$$

$$\ddot{\psi} = \frac{M_Z - F_X hs_\phi}{I_{zz}c_\phi^2 + I_{yy}s_\phi^2}, \tag{3}$$

$$I_{xx}\ddot{\phi} = F_Y hc_\phi + mghs_\phi + \dot{\psi}^2\Delta I_{yz}s_\phi c_\phi - K_\phi\phi - D_\phi\dot{\phi}, \tag{4}$$

$$F_X = F_x^f c_\delta + F_x^r - F_y^f s_\delta, \tag{5}$$

$$F_Y = F_y^f c_\delta + F_y^r + F_x^f s_\delta, \tag{6}$$

$$M_Z = l_f F_y^f c_\delta - l_r F_y^r + l_f F_x^f s_\delta, \tag{7}$$

where c_ϕ, s_ϕ are short for $\cos(\phi)$ and $\sin(\phi)$, and similarly for c_δ, s_δ. Further, m is the vehicle mass, h is the height of the center of mass, I_{zz} is the vehicle inertia about the z-axis, $\Delta I_{yz} = I_{yy} - I_{zz}$, $\dot{\psi}$ is the yaw rate, ϕ is the roll angle, δ is the steering angle measured at the wheels, v_x, v_y are the longitudinal and lateral velocities, l_f, l_r are the distances from the center of mass to the front and rear wheel base, F_x, F_y are the longitudinal and lateral forces acting on the front and rear wheels, and F_X, F_Y and M_Z are the resulting tire forces and moment. The roll dynamics is derived by assuming that the suspension system can be modeled as a spring-damper system—i.e., a dynamic system with stiffness K_ϕ and damping D_ϕ.

2.2 Wheel Modeling

The wheel dynamics is given by

$$T_i - I_w\dot{\omega}_i - F_x^i R_w = 0, \quad i = f, r. \tag{8}$$

Here, ω_i are the front and rear wheel angular velocities, T_i are the driving/braking torques, I_w is the wheel inertia, and R_w is the wheel radius. Slip angles α_f, α_r and slip ratios κ_f, κ_r are introduced following (Pacejka, 2006), and are described by

Table 1. Vehicle parameters used in (1)–(14).

Notation	Value	Unit
l_f	1.3	m
l_r	1.5	m
m	2 100	kg
I_{xx}	765	kgm^2
I_{yy}	3 477	kgm^2
I_{zz}	3 900	kgm^2
R_w	0.3	m
I_w	4.0	kgm^2
g	9.82	ms^{-2}
h	0.5	m
K_ϕ	178 000	Nm(rad)^{-1}
D_ϕ	16 000	Nms(rad)^{-1}

$$\alpha_f = \delta - \text{atan}\left(\frac{v_y + l_f\dot{\psi}}{v_x}\right), \tag{9}$$

$$\alpha_r = -\text{atan}\left(\frac{v_y - l_r\dot{\psi}}{v_x}\right), \tag{10}$$

$$\kappa_f = \frac{R_w\omega_f - v_{x,f}}{v_{x,f}}, \tag{11}$$

$$\kappa_r = \frac{R_w\omega_r - v_{x,r}}{v_{x,r}}, \tag{12}$$

$$v_{x,f} = v_x\cos(\delta) + (v_y + l_f\dot{\psi})\sin(\delta), \tag{13}$$

$$v_{x,r} = v_x. \tag{14}$$

The vehicle and wheel parameters used in this study are presented in Table 1.

The nominal tire forces—i.e., the forces under pure slip conditions—are computed with a simplified Magic Formula model (Pacejka, 2006), given by

$$F_{x0}^i = \mu_x F_z^i \sin(C_x^i\text{atan}(B_x^i\kappa_i - E_x^i(B_x^i\kappa_i - \text{atan}B_x^i\kappa_i))), \tag{15}$$

$$F_{y0}^i = \mu_y F_z^i \sin(C_y^i\text{atan}(B_y^i\alpha_i - E_y^i(B_y^i\alpha_i - \text{atan}B_y^i\alpha_i))), \tag{16}$$

$$F_z^i = mg(l - l_i)/l, \quad i = f, r, \text{ where } l = l_f + l_r. \tag{17}$$

In (15)–(17), μ_x and μ_y are the friction coefficients and B, C, and E are model parameters. Combined slip is modeled using the weighting functions presented in (Pacejka, 2006):

$$B_{x\alpha}^i = B_{x1}^i\cos(\text{atan}(B_{x2}^i\kappa_i)), \tag{18}$$

$$G_{x\alpha}^i = \cos(C_{x\alpha}^i\text{atan}(B_{x\alpha}^i\alpha_i)), \tag{19}$$

$$F_x^i = F_{x0}^iG_{x\alpha}^i, \tag{20}$$

$$B_{y\kappa}^i = B_{y1}^i\cos(\text{atan}(B_{y2}^i\alpha_i)), \tag{21}$$

$$G_{y\kappa}^i = \cos(C_{y\kappa}^i\text{atan}(B_{y\kappa}^i\kappa_i)), \tag{22}$$

$$F_y^i = F_{y0}^iG_{y\kappa}^i, \quad i = f, r. \tag{23}$$

In contrast to (15)–(23), a more complete form is presented in (Pacejka, 2006). However, since a single-track vehicle model is utilized here, the tire models have been recomputed such that they are symmetric with respect to the slip angle α and the slip ratio κ.

2.3 Tire-Force Characteristics and Model Calibration

In an optimal maneuver the tires are performing at their limits, thus implying the need for accurate tire modeling. Given a set of tire parameters for a nominal surface, (Pacejka, 2006) proposes to use scaling factors, λ_j, in (15)–(23) to describe different road conditions. This method was used in (Braghin et al., 2006), where the scaling factors representing surfaces corresponding to dry asphalt, wet asphalt, snow, and smooth ice were estimated based on experimental data. Since that study

included a set of different tire brands and models, the results presented could be seen as a general indication, or at least be used as guidelines, on how the tire characteristics will vary. We use the scaling factors from (Braghin et al., 2006) as a basis for calibrating tire models approximately corresponding to the force characteristics on the different surfaces. However, since the nominal tire parameters used in that paper are not public domain, we use the parameters from (Pacejka, 2006) to represent dry asphalt. The relative scaling factors, with respect to dry asphalt, are introduced according to

$$\lambda_{\text{dry}} = 1, \quad \lambda_{\text{wet}} = \frac{\lambda_{\text{wet}}^*}{\lambda_{\text{dry}}^*}, \quad \lambda_{\text{snow}} = \frac{\lambda_{\text{snow}}^*}{\lambda_{\text{dry}}^*}, \quad \lambda_{\text{ice}} = \frac{\lambda_{\text{ice}}^*}{\lambda_{\text{dry}}^*}, \quad (24)$$

where λ is the scaling factor used in this paper and λ^* is the scaling factor presented in (Braghin et al., 2006). Since a different set of nominal parameters are used, and since uncertainties in the estimation of the original scaling factors exist—especially for larger slip values—some inconsistent characteristics appear for the snow and ice models. The original snow model will produce a longitudinal force F_x that changes sign for large slip ratios, which is avoided by adjusting the scaling factor for C_x. For the ice model, multiple sharp and narrow peaks in the resultant force occur. This is adjusted by recomputing the scaling factor affecting (21), as well as the parameters B_{x2} and B_{y2}. In addition, the lateral curvature factor E_y is adjusted to smoothen the sharp peak originating from the relations in (15)–(16), which contributes to the inconsistencies in the resultant force. The complete set of tire model parameters used are provided in Table 2. Several of these parameters are dependent on the normal force F_z on the wheel. Hence, the front and rear parameter values differ—*e.g.*, the friction coefficients $\mu_{x,f}$ and $\mu_{x,r}$.

3. OPTIMAL CONTROL PROBLEM

The time-optimal hairpin maneuver problem is formulated as an optimization problem on the time-interval $t \in [0, t_f]$. The vehicle dynamics presented in the previous section is formulated as a differential-algebraic equation system (DAE) in the differential variables (states) x, algebraic variables y, and the

Table 2. Tire model parameters used to represent dry asphalt, wet asphalt, snow, and smooth ice.

Parameter	Dry	Wet	Snow	Ice
$\mu_{x,f}$	1.20	1.06	0.407	0.172
$\mu_{x,r}$	1.20	1.07	0.409	0.173
$B_{x,f}$	11.7	12.0	10.2	31.1
$B_{x,r}$	11.1	11.5	9.71	29.5
$C_{x,f}, C_{x,r}$	1.69	1.80	1.96	1.77
$E_{x,f}$	0.377	0.313	0.651	0.710
$E_{x,r}$	0.362	0.300	0.624	0.681
$\mu_{y,f}$	0.935	0.885	0.383	0.162
$\mu_{y,r}$	0.961	0.911	0.394	0.167
$B_{y,f}$	8.86	10.7	19.1	28.4
$B_{y,r}$	9.30	11.3	20.0	30.0
$C_{y,f}, C_{y,r}$	1.19	1.07	0.550	1.48
$E_{y,f}$	-1.21	-2.14	-2.10	-1.18
$E_{y,r}$	-1.11	-1.97	-1.93	-1.08
$C_{x\alpha,f}, C_{x\alpha,r}$	1.09	1.09	1.09	1.02
$B_{x1,f}, B_{x1,r}$	12.4	13.0	15.4	75.4
$B_{x2,f}, B_{x2,r}$	-10.8	-10.8	-10.8	-43.1
$C_{y\kappa,f}, C_{y\kappa,r}$	1.08	1.08	1.08	0.984
$B_{y1,f}, B_{y1,r}$	6.46	6.78	4.19	33.8
$B_{y2,f}, B_{y2,r}$	4.20	4.20	4.20	42.0

inputs $u = (T, \delta)$, according to $\dot{x} = G(x, y, u)$, and similarly for the tire dynamics, $h(x, y, u) = 0$. Introducing the maximum and minimum limits on the driving/braking torques and the steering angle, the mathematical optimization problem can be stated as follows:

$$\begin{align}
\text{minimize} \quad & t_f \tag{25} \\
\text{subject to} \quad & T_{i,\min} \leq T_i \leq T_{i,\max}, \; i = f, r \tag{26} \\
& |\delta| \leq \delta_{\max} \quad, \quad |\dot{\delta}| \leq \dot{\delta}_{\max} \tag{27} \\
& \left(\frac{X_p}{R_1^i}\right)^6 + \left(\frac{Y_p}{R_2^i}\right)^6 \geq 1 \tag{28} \\
& \left(\frac{X_p}{R_1^o}\right)^6 + \left(\frac{Y_p}{R_2^o}\right)^6 \leq 1 \tag{29} \\
& x(0) = x_0 \quad, \quad x(t_f) = x_{t_f} \tag{30} \\
& y(0) = y_0 \quad, \quad y(t_f) = y_{t_f} \tag{31} \\
& \dot{x} = G(x, y, u) \quad, \quad h(x, y, u) = 0, \tag{32}
\end{align}$$

where x_0, y_0 and x_{t_f}, y_{t_f} are the initial and final conditions, and (X_p, Y_p) is the position of the center-of-mass of the vehicle. The track constraint for the hairpin turn is formulated using two super-ellipses. In the implementation, the initial and final conditions are only applied to a subset of the variables.

The strategy for solving the optimal control problem is to use numerical methods for dynamic optimization. First, considering the setup of the hairpin turn, it can be concluded from a physical argument that existence of a solution is guaranteed. In this study, we utilize the open-source software JModelica.org (Åkesson et al., 2010), interfaced with the interior-point NLP-solver Ipopt (Wächter and Biegler, 2006), for solving the optimization problem. A direct collocation method (Biegler et al., 2002) is employed for discretization of the continuous-time optimal control problem. In order to achieve convergence in the NLP-solver, the hairpin turn problem is divided into smaller segments and thus solved in 4–8 steps sequentially, where the previous solution is used as an initial guess to the subsequent optimization problem. The final optimization solves the whole problem, thus not implying any suboptimality of the solution. From a numerical perspective, proper scaling of the optimization variables turned out to be essential for convergence. For details about the optimization methodology, the reader is referred to (Berntorp et al., 2013).

4. RESULTS

The optimization problem (25)–(32) was solved for each of the surface models presented in Sec. 2. The road was 5 m wide. The bounds on the driving/braking torques and tire forces were chosen as follows:

$$\begin{align}
& T_{f,\min} = -\mu_{x,f} F_z^f R_w \, , \; T_{f,\max} = 0, \tag{33} \\
& T_{r,\min} = -\mu_{x,r} F_z^r R_w \, , \; T_{r,\max} = \mu_{x,r} F_z^r R_w, \tag{34} \\
& |F_x^i| \leq \mu_{x,i} F_z^i, \tag{35} \\
& |F_y^i| \leq \mu_{y,i} F_z^i, \; i = f, r, \tag{36}
\end{align}$$

assuming that the vehicle is rear-wheel driven. Note that the bounds (35)–(36) on the forces were set for easier convergence, but are mathematically redundant. With the choice of the maximum driving/braking torques in (33)–(34), we introduce a dependency on the surface. This is motivated since the surface models adopted in this paper are only identified, and hence validated, for a certain region in the κ–α plane. Thus, allowing excess input torques might result in inconsistent behavior of the
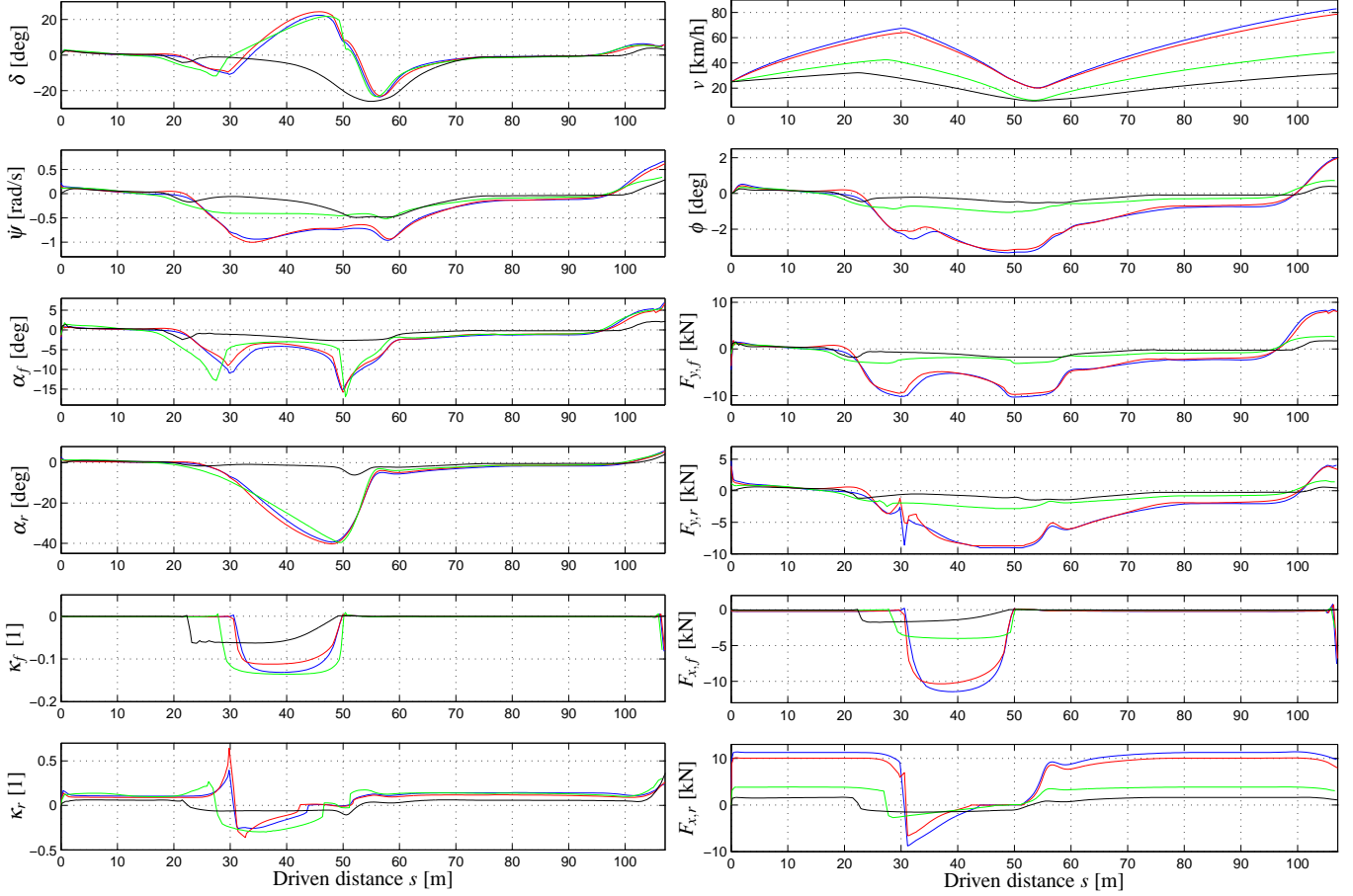
Fig. 3. Variables of the vehicle model during the time-optimal hairpin maneuver on the different surfaces, plotted as function of the driven distance s. The color scheme is as follows: dry asphalt–blue, wet asphalt–red, snow–green, and smooth ice–black.
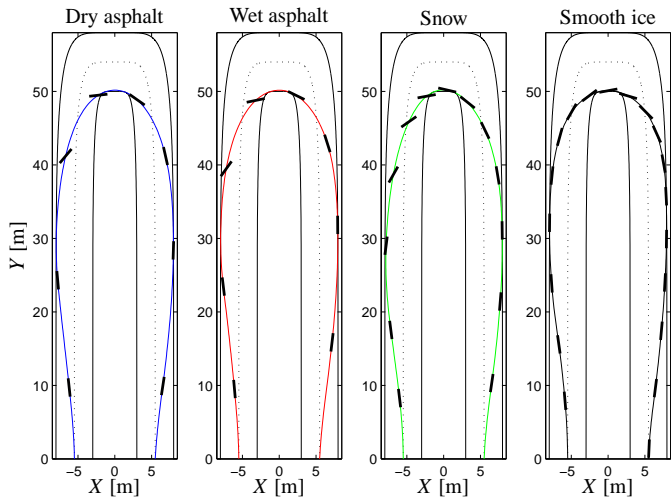

Fig. 4. Trajectory in the XY-plane for the different road surfaces. The black rectangles indicate the position and direction of the vehicle each second.

tire force model. Further, from a driver limitation argument the steering angle and steering rate were constrained according to

$$\delta_{\max} = 30 \text{ deg} \quad , \quad \dot{\delta}_{\max} = 60 \text{ deg/s}.$$

In addition, we constrained the wheel angular velocities ω_f, ω_r to be nonnegative—*i.e.*, the wheels were not allowed to roll backwards or back-spin.

With an initial velocity of 25 km/h, the results displayed in Fig. 3 are obtained. For comparison of the different surfaces, the model variables are visualized as function of the driven distance s instead of time. Further, the geometric trajectories corresponding to these control strategies are presented in Fig. 4. We also use the force–slip tire characteristic surfaces as a basis for analysis, as introduced in (Berntorp et al., 2013) and hereafter referred to as *Force-Slip (FS)-diagrams*. This 3D surface is defined as the resulting force

$$F_{i,\mathrm{res}} = \sqrt{(F_x^i)^2 + (F_y^i)^2}, \ i = f, r,$$

as function of the longitudinal slip κ and slip angle α. Plotting the optimal trajectory in this surface for both front and rear wheel, respectively, gives an effective presentation of the tire utilization in two plots, see Figs. 5–8. The time for execution of the maneuver is 8.48 s, 8.79 s, 13.83 s, and 19.18 s for dry asphalt, wet asphalt, snow, and smooth ice, respectively.

4.1 Discussion of Characteristics on Different Surfaces

The geometric trajectories of the vehicle center-of-mass, shown in Fig. 4, are close to each other for the different surfaces. This result might be unexpected, given the different surface characteristics. However, if comparing the paths for other parts of the vehicle, such as the front or rear wheel, more pronounced differences are seen as a result of the different slip behavior. Obviously, the time for completing the maneuver is longer for the snow and ice surfaces than for asphalt. This is a result of the tire forces that can be realized on these surfaces. Further, the
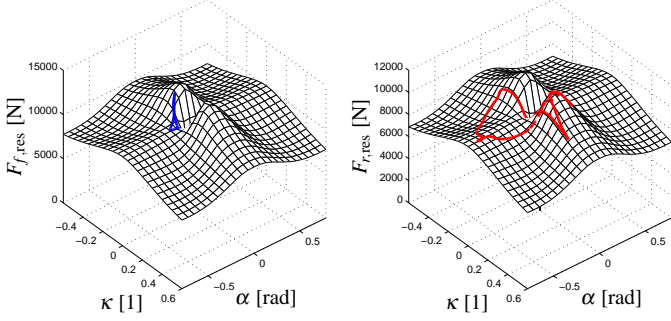
Fig. 5. The resulting tire forces for the dry asphalt model. The front tire force is shown in blue and the rear tire force is shown in red. The rear tire force exhibits more variation, caused by the vehicle being rear-wheel driven.
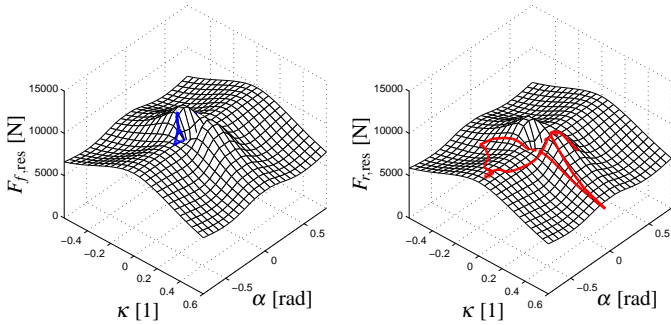

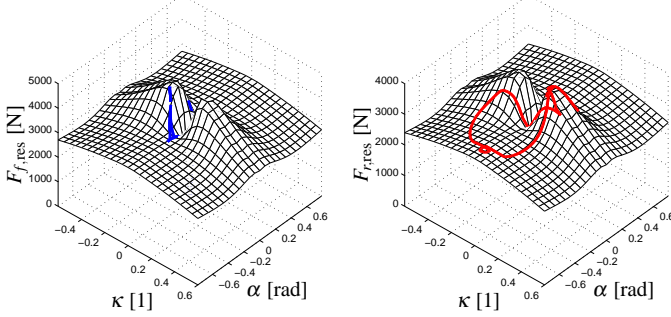Fig. 6. The resulting tire forces for the wet asphalt model.

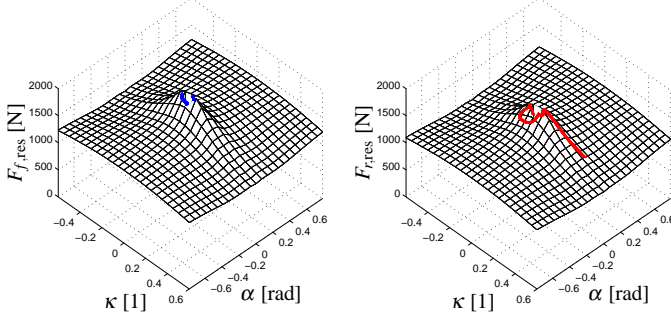Fig. 7. The resulting tire forces for the snow model.

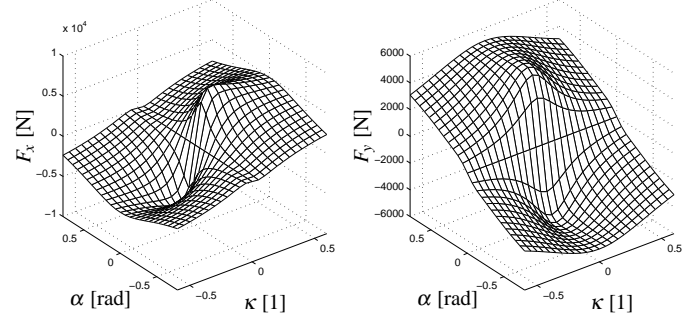Fig. 8. The resulting tire forces for the smooth ice model.

Fig. 9. Front tire forces in the longitudinal and lateral wheel directions for dry asphalt, corresponding to Fig. 5.
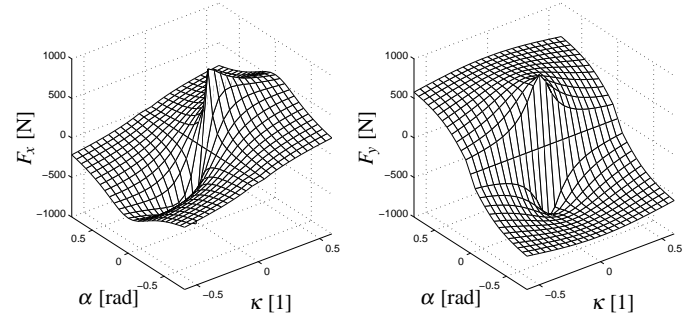

Fig. 10. Front tire forces in the longitudinal and lateral wheel directions for ice, corresponding to Fig. 8.

means that combined slip yields a significantly smaller resultant force. Thus, to achieve the desired time-optimality on the ice surface, it is natural to choose a small-slip control strategy.

Comparison of Control Strategies The internal variables of the vehicle model during the maneuver, see Fig. 3, are similar for dry and wet asphalt. The similarity is expected, considering the tire force characteristics in the two cases. As anticipated, the major difference between the two surfaces is the time for execution of the maneuver, which is slightly longer for the wet asphalt surface. This is expected since the maximum tire forces are lower than for dry asphalt.

The differences between asphalt, snow, and ice when considering the control strategy are fundamental. First, it can be concluded that the optimal maneuver on snow and ice surfaces are more proactive in the sense that both the steering angle δ and braking forces are applied considerably earlier when approaching the hairpin. This is most certainly an effect of the significantly reduced tire forces that can be realized on these surfaces compared to asphalt. The steering angle also differs between ice and the other surfaces. The reason for this is that the vehicle employs counter-steering when it starts to slip on asphalt and snow as it approaches the hairpin. Further, we see that the roll angle is considerably smaller for the low-friction surfaces, which is caused by the torque about the roll axis (produced by the tire forces) being smaller. Moreover, even on dry asphalt the roll angle is kept below approximately 3.2 deg, verifying that no unstable modes are excited. The slip ratio κ differs in amplitude between the road-surfaces. The reason becomes clear when investigating the FS-diagrams and the corresponding tire utilization, Figs. 5–8. The peak of the resultant force in the κ–α plane occurs at smaller slip values for ice, which implies a control solution with smaller slip angles for minimum-time.

vehicle exhibits large slip in the critical part of the maneuver on all surfaces except smooth ice. The reason for this difference becomes evident when examining the force characteristics of the smooth ice model compared to, *e.g.*, the dry asphalt model. In Figs. 9 and 10 the longitudinal and lateral tire forces are shown for these surfaces, *cf.* Figs. 5 and 8. The tire forces for smooth ice exhibit a considerably sharper peak and thus decay faster, with respect to combined slip, than for dry asphalt. This
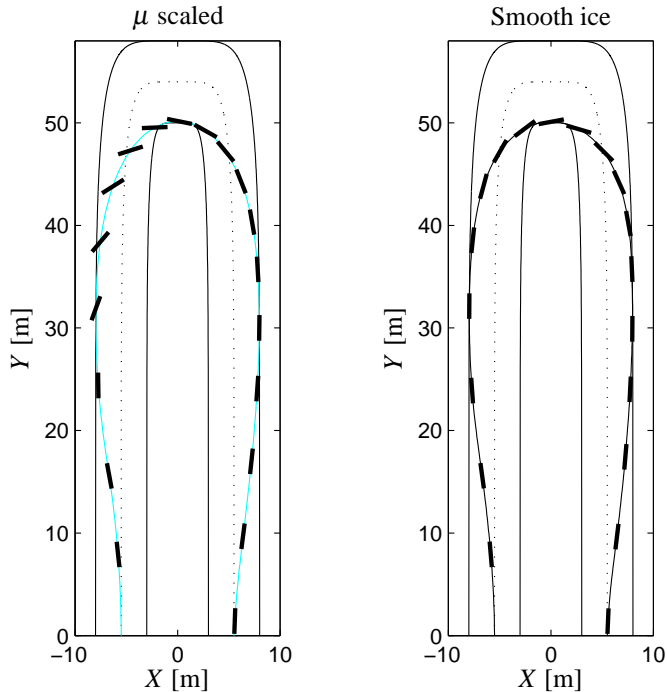
Fig. 11. Optimal hairpin maneuver on ice for two tire model parametrizations: Scaling of friction coefficients (left) and empirical tire model (right). Scaling of μ only renders an optimal solution with large slip.

Discussion on Tire Model Calibration An integral part of the vehicle model is the tire characteristics. Consequently, different approaches to model calibration were investigated prior to the study. One approach would be to only scale the friction coefficients μ_x and μ_y, as done in (Chakraborty et al., 2011). However, the peaks in the tire-force surfaces occur at different lateral and longitudinal slip combinations, see Figs. 5–8. Also, the sharpness and width of the maxima and minima change for the different models. Thus, only changing the friction coefficients will render different force characteristics—and thus different optimal solutions—compared to when changing the complete set of parameters. This is verified by constructing a tire force model where the dry asphalt parameters are used together with the friction coefficients corresponding to ice. Performing the optimization gives that the optimal solution has significant slip, on the contrary to the results obtained for the empirical smooth-ice model; see Fig. 11 for the results obtained by scaling the friction coefficients only. Another approach to tire model calibration is to scale the slip stiffness (*i.e.*, the parameters B_x and B_y in (15)–(17)) in addition to the friction coefficients. This will change both the inclination and the slip value where the maximum tire force is attained. However, adjusting these parameters without considering the parameters corresponding to combined slip will, in this case, result in multiple sharp and narrow peaks in the resultant force, which might be unrealistic from a physical point-of-view.

5. CONCLUSIONS

Optimal vehicle maneuvers under varying road conditions give valuable insight into the dynamics when the vehicle performs at the limit. One observation was that tire-force modeling on different road surfaces using only a scaling of the friction coefficients is insufficient for the maneuver considered, at least when the tires perform at their limits. Rather, when combined longitudinal and lateral slip is present, more careful tire modeling may be required. The minimum-time hairpin maneuver, using tire models representing different road surfaces, gave as a first major observation that the path through the turn was almost the same independent of different road-surface characteristics, such as dry asphalt or ice. Of course, the total execution time is longer on ice than asphalt, but there are also other differences which lead to the second major conclusion: The optimal driving techniques—*i.e.*, the control actions—are fundamentally different depending on tire-road characteristics. This is an important finding since it implies that in order to enjoy the full benefits of improved sensor information, future safety systems will need to be more versatile than systems of today. Further, that the path of the vehicle center-of-mass is almost invariant gives inspiration to look for strategies based on path formulations when approaching the goal of developing new model-based vehicle safety systems more robust to road-surface uncertainties.

REFERENCES

Åkesson, J., Årzén, K.E., Gäfvert, M., Bergdahl, T., and Tummescheit, H. (2010). Modeling and optimization with Optimica and JModelica.org—Languages and tools for solving large-scale dynamic optimization problems. *Computers and Chemical Engineering*, 34(11), 1737–1749.

Berntorp, K., Olofsson, B., Lundahl, K., Bernhardsson, B., and Nielsen, L. (2013). Models and methodology for optimal vehicle maneuvers applied to a hairpin turn. In *Am. Control Conf. (ACC)*. Washington, DC.

Biegler, L.T., Cervantes, A.M., and Wächter, A. (2002). Advances in simultaneous strategies for dynamic process optimization. *Chemical Engineering Science*, 57, 575–593.

Braghin, F., Cheli, F., and Sabbioni, E. (2006). Environmental effects on Pacejka's scaling factors. *Vehicle System Dynamics: Intl. J. Vehicle Mechanics and Mobility*, 44(7), 547–568.

Chakraborty, I., Tsiotras, P., and Lu, J. (2011). Vehicle posture control through aggressive maneuvering for mitigation of T-bone collisions. In *IEEE Conf. on Decision and Control (CDC)*, 3264–3269. Orlando, FL.

Funke, J., Theodosis, P., Hindiyeh, R., Stanek, G., Kritatakirana, K., Gerdes, C., Langer, D., Hernandez, M., Muller-Bessler, B., and Huhnke, B. (2012). Up to the limits: Autonomous Audi TTS. In *IEEE Intelligent Vehicles Symp.*, 541–547. Alcalá de Henares, Spain.

Isermann, R. (2006). *Fahrdynamik-Regelung: Modellbildung, Fahrerassistenzsysteme, Mechatronik*. Vieweg-Verlag, Wiesbaden, Germany.

Kelly, D.P. and Sharp, R.S. (2010). Time-optimal control of the race car: a numerical method to emulate the ideal driver. *Vehicle System Dynamics*, 48(12), 1461–1474.

Kiencke, U. and Nielsen, L. (2005). *Automotive Control Systems—For Engine, Driveline and Vehicle*. Springer-Verlag, Berlin Heidelberg, second edition.

Lundahl, K., Berntorp, K., Olofsson, B., Åslund, J., and Nielsen, L. (2013). Studying the influence of roll and pitch dynamics in optimal road-vehicle maneuvers. In *23rd Intl. Symp. on Dynamics of Vehicles on Roads and Tracks (IAVSD)*. Qingdao, China.

Pacejka, H.B. (2006). *Tyre and Vehicle Dynamics*. Butterworth-Heinemann, Oxford, United Kingdom, second edition.

Sharp, R.S. and Peng, H. (2011). Vehicle dynamics applications of optimal control theory. *Vehicle System Dynamics*, 49(7), 1073–1111.

Sundström, P., Jonasson, M., Andreasson, J., Stensson Trigell, A., and Jacobsson, B. (2010). Path and control optimisation for over-actuated vehicles in two safety-critical maneuvers. In *10th Intl. Symp. on Advanced Vehicle Control (AVEC)*. Loughborough, United Kingdom.

Velenis, E. and Tsiotras, P. (2005). Minimum time vs. maximum exit velocity path optimization during cornering. In *IEEE Intl. Symp. on Industrial Electronics (ISIE)*, 355–360. Dubrovnik, Croatia.

Velenis, E. (2011). FWD vehicle drifting control: The handbrake-cornering technique. In *IEEE Conf. on Decision and Control (CDC)*, 3258–3263. Orlando, FL.

Wächter, A. and Biegler, L.T. (2006). On the implementation of an interior-point filter line-search algorithm for large-scale nonlinear programming. *Mathematical Programming*, 106(1), 25–57.